Photovoltaics in Van der Waals Heterostructures

Marco M. Furchi, Armin A. Zechmeister, Florian Hoeller, Stefan Wachter, Andreas Pospischil, and Thomas Mueller

(Invited Paper)

***Abstract*—The peculiar nature of light-matter interaction in atomically thin transition metal dichalcogenides is recently under examination for application in novel optoelectronic devices. Here, we show that heterostructures composed of two or more such layers can be used for solar energy harvesting. The strong absorption in these atomically thin layers makes it possible to achieve an efficient power conversion with a minimal amount of active material. We describe in detail two different fabrication techniques that allow to realize heterostructures with clean, atomically sharp interfaces. The observed electrical and photovoltaic properties are analyzed. Our findings suggest that, accompanied by the advances in large area fabrication of atomically thin transition metal dichalcogenides, van der Waals heterostructures are promising candidates for a new generation of excitonic solar cells.**

***Index Terms*—excitonic solar cells, MoS2, MoSe2, WSe2, TMDs, van der Waals heterostructures.**

I. Introduction

FIRST investigations on the optical properties of transition metal dichalcogenides (TMDs) were preformed already back in the 1960s [1]–[3]. These materials were known to exist in a layered structure. Each TMD layer is composed of a sheet of transition metal atoms (M) in between two sheets of chalcogene (X) atoms. Whereas the bonding within an X-M-X monolayer is covalent, the bonding between individual layers is due to van der Waals forces. This unique property allowed the preparation of thin crystals by cleaving using adhesive tape. The acquired absorption spectra were dominated by peaks arising from strong excitonic absorption. This was attributed to the confinement of the excitons due to the two-dimensional character of the materials. The exciton binding energy of a truly two-dimensional exciton was predicted to be four times the three-dimensional value [4].

Driven by the hope of finding new extremal states of matter that could arise from the two-dimensional character of these layered crystals, experiments on a wide range of diverse topics were performed. Exciton screening, Bose-Einstein condensations, exciton superfluidity as well as the insulator/metal transition and superconductivity were a few among these [5]. In the late 70s, TMDs were used as electrodes of photoelectrovoltaic cells. Their bandgaps, that match well with the solar spectrum, as well as the covalent layer-type nature of these compounds made them promising candidates for efficient solar energy conversion. Solar to electrical power conversion efficiencies up to 10.2% were achieved using tungsten diselenide (WSe_2) and molybdenium disulfide ($MoSe_2$) crystals [6]. The photovoltaic effect arising from Schottky barriers of metals on natural p-type MoS_2 [7] and other TMDs [8] were investigated and an efficient conversion of solar energy was demonstrated.

Cleaved surfaces of TMDs have no dangling bonds. Thus, heterostructures with a large lattice mismatch can be formed. Motivated by the advances in molecular beam epitaxy (MBE) Koma *et al.* managed to grow the first two-dimensional NbSe layer in 1984 [9]. In a later work, the first growth of a two-dimensional material on a three-dimensional material was achieved [10]. Apart from this MBE based method, named "van der Waals epitaxy" [11], ultra-thin layers of TMDs were grown on amorphous substrates by "reactive van der Waals rheotaxy" [12]. To our knowledge, these artificially grown two-dimensional layers were never examined in terms of optical and electrical properties.

More recently, the work on graphene [13] and other two-dimensional crystals [14], by Geim *et al.*, has led to renewed interest in atomically thin materials. Atomically thin semiconducting TMDs were found to have unique optical properties and thus a high potential for novel optoelectronic devices. Not only traditional semiconductor devices, like photodetectors, light emitting diodes and solar cells, but also single photon emitters and valleytronic devices were demonstrated [15]. Unlike their bulk counterparts, TMD monolayers show a direct bandgap [16]. Furthermore, exciton binding energies were found to be increased not only due to the geometrical confinement, but also due to the reduced dielectric screening [17]. For single layers of semiconducting TMDs the binding energies were found to range up to 700 meV [18]. Simulation results indicate that this extraordinary strong binding leads to an increase of the absorbance at visible energies by a factor of $\approx$2 [19]. A monolayer of molybdenum diselenide ($MoSe_2$) (with a thickness of 0.65 nm) absorbs the same fraction of light as 15 nm of gallium arsenide (GaAs) or 50 nm of silicon (Si). This can be explained by additionally taking into account dipole transitions with large joint density of states, as well as the oscillator strengths between localized d-states with strong spatial overlap [19].

Manuscript received April 7, 2016; revised June 14, 2016; accepted June 14, 2016. Date of publication June 20, 2016; date of current version September 6, 2016. This work was supported by the Austrian Science Fund FWF (START Y-539) and the European Union Seventh Framework Programme under Grant 604391 Graphene Flagship.

The authors are with the Photonics Institute, TU Wien, Vienna 1040, Austria (e-mail: marco.furchi@tuwien.ac.at; armin.zechmeister@tuwien.ac.at; florian.hoeller@tuwien.ac.at; stefan.wachter@tuwien.ac.at; andreas.pospischil@tuwien.ac.at; thomas.mueller@tuwien.ac.at)

Color versions of one or more of the figures in this paper are available online at http://ieeexplore.ieee.org.

Digital Object Identifier 10.1109/JSTQE.2016.2582318

Conversion of optical in to electrical energy consists of three processes: light absorption causing a transition from a ground state into an excited state, conversion of the excited state into free charge carriers and a discriminating transport mechanism [20]. The high absorbance given by the unique nature of absorption processes in TMD monolayers is one of the properties that make them promising candidates for crystalline ultra-thin solar cells.

The highest power conversion efficiencies achieved so far were demonstrated using mono-crystalline cells. But such solar cells are only used if high efficiency is the central requirement and costs play a secondary role. Nevertheless, for commercial applications a reduction of material consumption and costs is necessary. Therefore, driven by the advances in efficient thin-film fabrication, recent work focuses on ultra-thin mono-crystalline solar cells [21]. Additionally, thin devices have one further intrinsic advantage. Due to the reduced thickness, one of the major efficiency limiting factors, namely charge separation prevented by electron-hole recombination, is strongly diminished [22]. Recently, it was demonstrated that the potentially highest conversion efficiencies can be obtained by using ultra-thin absorbers and reflective back scattering layers [23]. The optimal thickness for a GaAs solar cell was calculated to be 15 nm and the theoretical efficiency limit for such a solar cell was found to be 17% [22]. This further highlights the potential of atomically thin TMD layers regarding their use for photovoltaic energy conversion.

One viable strategy for increasing the power conversion efficiency is the combination of multiple materials with distinct bandgaps. Thereby, the amount of absorbed energy is maximized and concurrently the energy loss due to the relaxation of the excited carriers is minimized. IV and III-V semiconductors span a wide range of bandgaps, ranging from 0.35 eV for indium arsenide (InAs) to 2.5 eV for aluminum phosphide (AlP) [24]. Nevertheless, only materials whose lattice constant differs by less than 2% can be combined to form a heterostructure. This strongly limits the number of possible combinations. As TMD layers are bound by weak van der Waals forces, even twisted layers can be combined to form heterostructures with atomically sharp junctions.

Inspired by the huge potential of atomically thin TMDs outlined above, we designed and fabricated multiple van der Waals heterostructure-based solar cells. In this paper we present an extended study of the properties of these cells. Section II describes the device design and fabrication. Section III discusses the experimental findings and our theoretical interpretation. Section IV summarizes our findings and proposes further experiments that could lead to efficient van der Waals heterostructure based photovoltaics.

II. Device Structure and Fabrication

As mentioned earlier, the photovoltaic properties of bulk TMDs were already explored more than five decades ago. The demonstrated devices showed high power conversion efficiencies. Nevertheless, regarding an eventual commercial application the efficiency is not the only relevant factor. Module lifetimes, manufacturing and installation costs, as well as the environmental impact of the manufacturing and the deployment have to be taken into account. The last three can be accounted for as the "true costs" of the solar cell module. Including all the named factors, a better figure of merit can be defined as FOM $= [\,\text{energy conversion efficiency} \,/\, \text{true costs}\,] \times \text{lifetime}$ [25]. With this in mind, it is evident that both mentioned devices realized with bulk TMDs have major drawbacks. Schottky junction solar cells suffer from the small active area making an upscaling infeasible, and the working principle of photoelectrochemical cells leads to the corrosion of the active material strongly limiting the lifetime of such devices. Thinning down TMDs to their monolayer form has a strong impact on their properties. These properties were first explored, in terms of solar energy conversion, by fabricating p-n junctions in split gate configurations [26], [27]. A conversion of optical into electrical energy was demonstrated. Nevertheless, like for Schottky junction cells, the potential for an application of such devices for solar energy harvesting is strongly limited by the scalability of the active region. This area is limited because in one lateral dimension the size must be optimized while taking into account the following trade off: a longer p-n junction decreases the efficiency of charge separation and simultaneously increases the active area. The maximal length is therefore less than a few micrometers. In the other dimension the size is given by the width of the used TMD crystal. The so achieved power conversion efficiencies were found to be about 0.5% and limited due to interlayer recombination processes.

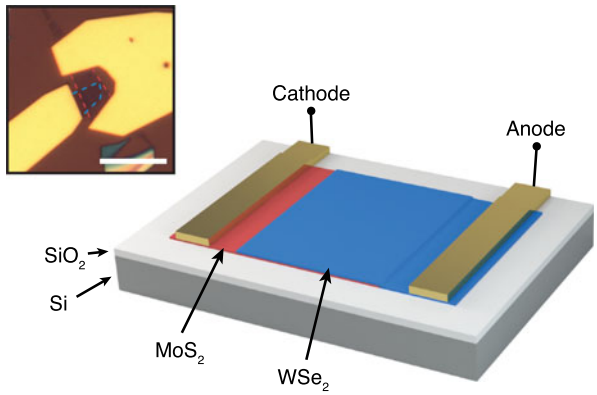

Fig. 1. Three dimensional schematic view of the dual bandgap cells. Inset: Optical micrograph of one dual bandgap device. The outer edges of the TMD flakes are indicated by the dashed lines (red and blue for MoS_2 and WSe_2 respectively). The scale bar is 10 μm.

To realize a solar cell with scalable active region, the separation of charge carriers upon absorption has to arise from an effect that can effectively act on large areas. One option is to form a vertical p-n junction. In such a structure the discriminating transport mechanism arises from a built-in field created by the p-n junction. One other option is a vertical type-II heterostructure. If the exciton binding energies are high and thus their lifetime is long, excitons can diffuse to the interface where they are dissociated. As the charge carriers relax to the energetically lowest levels, electrons and holes end up in different materials. This dissociation and separation produces a chemical potential energy gradient that drives the photovoltaic effect

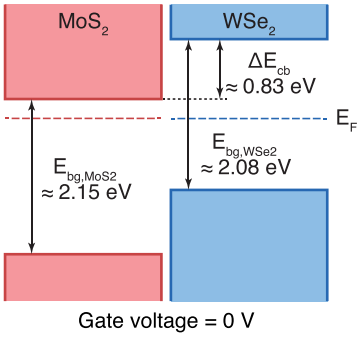

Fig. 2. Schematic diagram of the band alignment in a dual bandgap heterostructure; The expected alignment of the Fermi energy, valence band maxima and conduction band minima in a MoS_2 – WSe_2 heterostructure.

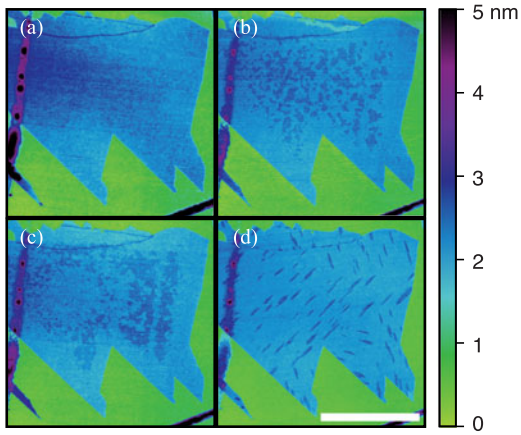

Fig. 3. Effect of high vacuum annealing; Atomic force micrographs of a contaminated WSe_2 flake after annealing at 95 °C for (a) 0 h (b) 25 h (c) 35 h (d) 40 h. The scale bar is 4 μm.

even in absence of a built-in electrical field [28]. Theoretical predictions indicate that TMDs combined into a vertical van der Waals junction form such a type-II heterostructure [29], [30]. The size of the active area of such a device is in principle only limited by the dimension of the layers forming the junction.

A. *Dual Bandgap Heterostructure*

The first kind of devices we fabricated, namely double bandgap van der Waals heterostructures, were made by stacking two atomically thin TMD layers. Fig. 1 shows a schematic of the dual bandgap devices. The optical band gaps of MoS_2 and WSe_2 are known to be 1.85 eV [31] and 1.65 eV [32], respectively. Although, the optical band gaps of these two materials may not be ideal for a double band gap solar cell, we chose these materials because of their availability and the predicted type II band alignment that is crucial for photovoltaic energy conversion [33]. A sketch of the expected band-structure is shown in Fig. 2.

For the fabrication of the devices, at first the lower TMD flakes were exfoliated onto a silicon wafer dice covered by 285 nm dry thermal silicon dioxide (SiO2). The thickness of the oxide was chosen to be such that the contrast of thin layers found on its surface is enhanced. The exfoliation was done as follows: first a thick TMD crystal was pre-cleaved a few times using multiple adhesive tape stripes. The prepared tape with a thin TMD crystal was put aside while the wafer dices were cleaned in an ultrasonic acetone bath followed by a dip in isopropyl alcohol (IPA) and blow-drying with nitrogen. Then the tape was placed on the wafer dice and subsequently peeled off by a continuous slow motion. The mono-layer flakes were preselected by optical microscopy. This can be done with a high success rate because the contrast of thin flakes depends on the layer number. Thereafter, the thickness of the preselected flakes was verified by photoluminescence and Raman measurements. As the cleanliness of the single layers is crucial for the formation of a good, trap-free interface, the substrates were thermally annealed for 8 hours in vacuum (at a pressure below 5×10^{-6} mbar). Thermal annealing is known to reduce the amount of residues on-top of atomically thin layers [34]. To prove the reduction of adsorbate contaminated area by our annealing process, a WSe2 flake with a large amount of adsorbates was annealed and imaged at different time periods using an atomic force microscope. Fig. 3 illustrates the increase of clean surface area due to the annealing process. While in the first subfigure (Fig. 3(a)) the contaminated area is large and the residues are evenly distributed, the last subfigure (Fig. 3(c)) shows a clustering of the residues. By the concentration of the adsorbates on small islands and a partial desorption of the residues the clean surface area is strongly increased. Still, it has to be noted that the heterostructures were fabricated using flakes with a far lower amount of adsorbates. Interestingly the needle shaped islands formed by the residues appear to have three preferred directions. As these show a rotation angle of 60° in respect to each other, we believe that their orientation is related to the crystal structure of the flake.

For the upper TMD flakes the exfoliation was done as described above but on a silicon wafer dice covered by a stack of a water soluble polymer (polyacrylic acid, PAA) coated by an acetone soluble, strongly hydrophobic polymer (poly methyl pethacrylate, PMMA). The thickness of both layers was adjusted such that the contrast of atomically thin layers on the surface of the PMMA layer strongly increased, the PAA layer was thick enough to enable a complete dissolution and the PMMA layer was mechanically stable to withstand the subsequent fabrication steps.

To build the heterostructure, the PMMA layer carrying the upper flake was released from the sacrificial silicon substrate by dissolving the PAA layer in a water bath. The PMMA layer was then transferred onto a microscope slide and the microscope slide was turned upside down. Then, by using a micromechanical triaxial stage, the upper flake was precisely positioned on-top of the lower one. This was done on a heatable platform, which after positioning was heated up to about 110 °C (slightly above the glass transition temperature of PMMA). Due to the heat the PMMA layer softened and strongly adhered to the silicon substrate. After cooling down the wafer dice was put into a deep-ultraviolet light exposure chamber for 4 to 8 hours. This lead to a breaking of the polymer chains into shorter ones, making the PMMA layer less chemically stable [35]. By doing so, the mechanical stress on the TMD flake during the dissolution of the PMMA layer was strongly reduced. The dis-

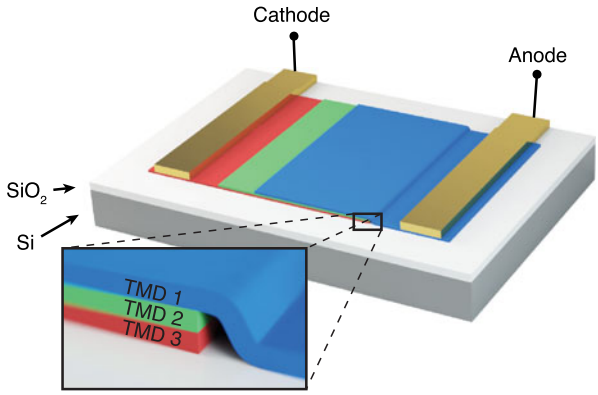

Fig. 4. Three dimensional schematic view of a triple bandgap cell. The TMDs used in our cells were WSe_2, WS_2 and MoS_2.

solution was done by placing the whole sample into an IPA-filled flat petri dish and slowly adding acetone until the appropriate concentration was reached (the PMMA layer slowly starts to dissolve). After the stacking process was finalized the sample was again annealed for 8 hours at 100 °C in vacuum (below 5×10^{-6} mbar).

Using electron beam lithography, a PMMA evaporation mask for the contacts was made. Then, by electron beam evaporation in vacuum at low base pressure (below 2×10^{-7} mbar) one 6 nm thick adhesion promoting layer of titanium and subsequently one 80 nm thick contact layer of gold were evaporated. To finalize the device, lift off was done in an acetone bath (heated up to 64 °C) and the wafer-dice was annealed one last time for 8 hours at 100 °C in vacuum (below 5×10^{-6} mbar). An optical microscope image of one double bandgap heterostructure device is shown in the inset of Fig. 1.

B. Triple Bandgap Heterostructure

The second kind of devices, namely triple bandgap van der Waals heterostructures, consist of a stack of three atomically thin TMD layers (see Fig. 4). The materials used for these devices were MoS_2, WS_2 and WSe_2 (WS_2 has an optical band gap of 2.0 eV [36]). If clean interfaces are needed, the method described above only allows the stacking of two flakes, because of polymer residues left on top of the flakes. To circumvent this the following method was used.

Single TMD flakes were exfoliated on SiO_2 covered Si-Wafers. Again, they were preselected using optical microscopy, their thickness was confirmed spectroscopically and the flakes were thermally annealed in vacuum (below 2×10^{-7} mbar) for 8 hours at 100 °C. This second method allows to peel off single TMD flakes by exploiting the fact that van der Waals forces between two TMD layers are stronger than between one TMD layer and the SiO2 surface.

Polydimethylsiloxane (PDMS) is a viscoelastic, optically clear, polymeric compound, commonly referred to as silicone. Although PDMS can be directly used to pick up small objects from one surface and release them on another [37], [38] it was found to leave residues. The removal of these oligomers (monomers that can be found on the surface of fully cross-linked PDMS) involves aggressive chemicals that may interact with the transferred TMD flakes. Therefore, the pick-and-place method had to be modified by adding a second polymer layer. A thermoplastic polymer was placed on-top of the PDMS stamp. The PDMS layer served as transparent elastic layer that allowed to uniformly apply a force on the thermoplastic polymer. The thermoplastic layer was used to pick up the uppermost flake of the TMD stack (e.g., TMD1 in Fig. 4). This was done by bringing the polymer in contact with the TMD flake and the SiO_2 substrate. Then the substrate was heated to a temperature above the glass transition temperature of the polymer. Thereby, it conformally embeded the TMD flake. After cooling down, the van der Waals forces in-between the polymer and the TMD flake were greater than those that bind the TMD flake to the SiO_2 surface. Hence, by peeling off the polymer, the TMD flake was also peeled off the substrate. Despite, most groups use polycarbonate (PC) as thermoplastic polymer layer, we decided to use polypropylene carbonate (PPC) instead because it has a far lower glass transition temperature, not only reducing an eventual thermally driven degradation of the TMD flakes, but also facilitating the dissolution of the PPC layer after finalizing the stack.

About 1 mm thick PDMS layers were prepared using commercially available Sylgard 184 Silicone. We used a 20:1 mixture of PDMS base:curing agent. Air inclusion arising form the mixing process of PDMS base and curing agent was removed using a centrifuge. Finally, after pouring the mixture into a petri dish to form 1 mm thick layers, curing at 48 °C for 6 hours was performed. PPC was dissolved in chloroform (1:20). A thin layer was formed on a microscope slide by dropping about 200 μl of the solution onto it and subsequently sliding another slide over it. A 2×2 mm large piece was cut out of the PDMS layer and placed onto a clean microscope slide. The PPC layer was peeled off the microscope slide and transferred onto the slide with the small PDMS dice, in a way that it also covers a large area of the microscope slide.

To pick up the first TMD flake, the wafer dice carrying it was placed on a platform heated up to about 68 °C. Then, using a micro mechanical stage, the microscope slide with the polymer stack was brought into contact with the sample. This was done such that the TMD flake to pick up was aligned in the center of the PDMS dice. After cooling the platform down to 20 °C, the microscope slide was lifted up again. Thereby, the TMD flake was transferred from the SiO_2 surface to the polymer. We found that by preheating the sample, the probability of picking up the first flake strongly increased. As the yield for the subsequent pick up of additional TMD flakes (e.g., TMD2 in Fig. 4) was close to 100% no preheating was necessary. Thus, we were able to align both flakes with a higher precision and even realign if mispositioned. To finalize the stack, the picked-up flakes were released onto the lowermost flake. This was done by again aligning and bringing into contact the flakes and subsequently heating up the platform to about 120 °C. Then, while keeping the platform at this temperature, the microscope slide was lifted up. By that, the upper half of the PPC sticked on the PDMS whereas the lower part remained on the substrate. The removal of the PPC layer was done by heating up the wafer

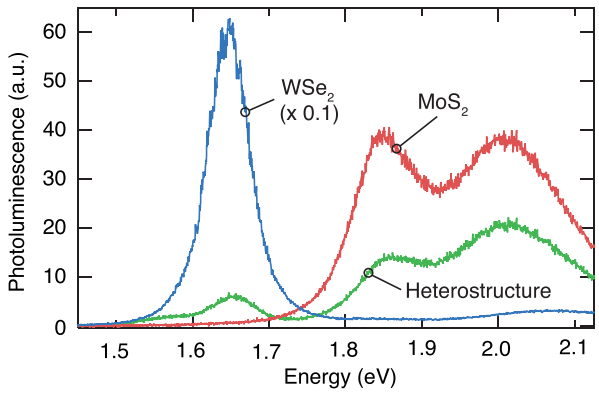

Fig. 5. Photoluminescence spectra recorded at different positions on the sample.

dice to 62 °C and placing it into a chloroform bath that was also kept at 62 °C for 5 minutes. We observed that dissolving the PPC layer in cold chloroform often lead to a delamination of the TMD stack.

As for the double band gap van der Waals heterostructure devices, the flakes were finally contacted by means of standard electron beam lithography processes. Again, a final thermal annealing step at 100 °C in vacuum was done.

III. Experimental Results and Discussion

In the first part of this section we focus on the properties of the dual bandgap heterojunction cell. In the second part we describe the properties of the triple bandgap heterojunction cell.

A. Dual Bandgap Heterostructure

Photoluminescence spectroscopy is a powerful tool to study the optical properties of semiconductors. In most semiconducting TMDs a transition from indirect to direct gap semiconductor by thinning crystals down to monolayer thickness was predicted and observed [16], [31], [32]. The corresponding increase of photoluminescence efficiency can be used to identify atomically thin flakes. Fig. 5 shows our measurements on three different locations on our device. The measurements were performed at room temperature by exciting the samples with a 532 nm solid state laser. The response measured on the single layers correspond to the spectra found in literature [16], [31], [32]. For WSe_2 we find a strong excitonic resonance peaking at 1.65 eV. The measurement of the MoS_2 flake shows two peaks (A and B exciton) at 1.85 and 2.1 eV. In the region in which the WSe_2 flake overlaps with the MoS_2 flake, the photoluminescence cannot be explained by a simple superposition of the single layer spectra. Other than that, a strong quenching of the luminescence is observed. This indicates that a new non-radiative recombination path at lower energies arises from the stacking. Consequently, a strong interlayer coupling can be assumed. Additionally, the measurement shows that the MoS_2 emission is reduced by $\sim$65%, whereas the WSe_2 emission shows a reduction of $\sim$98%. A strong interlayer coupling in a type-I heterostructure would lead to an eventual increase of the luminescence stemming from the lower bandgap material accompanied by a reduction of the emission from the higher bandgap material. Thus, our result strongly supports the assumption of type-II band alignment. Taking into account the high exciton binding energies in monolayer TMDs additionally indicates that the electrical heterojunction bandgap is smaller than the optical bandgaps of both materials.

Recent measurements on the band profiles of single layer MoS_2 and WSe_2 [39] support our findings. A type-II alignment was confirmed. The valence band offset was found to be about 0.83 eV. The electric bandgap was measured to be 2.15 and 2.08 eV for MoS_2 and WSe_2, respectively. In addition, it should be noted that other reports show a strong emission arising from a heterojunction bandgap [40]–[42]. It was shown that even small twist angles strongly quench this emission. As we did not put any effort into aligning the lattice orientation, we suppose that the lack of this feature in our spectra arises from a misalignment of the TMD flakes.

Most conventional semiconductor solar cells consist of planar large area p-n homojunctions. The doping of the semiconductors is achieved by intentionally introducing impurities. At the interface of the p- and n- doped regions a depletion zone forms. This results in a discriminative mechanism that leads to opposite transport directions for charge carriers of opposite polarities. In effect, a rectifying behavior and a net current upon illumination can be observed. The situation is different for van der Waals heterostructures. Due to the atomically sharp transition no depletion zone is formed. Instead, the interface can be seen as a potential barrier. Its width is given by the interlayer spacing of the van der Waals bound layers and the height approximately corresponds to the work function of the materials. Fig. 2 presents the band diagram of our structure at zero gate and bias voltage. The only possible pathway for charge carriers to move across the junction is by tunneling across the barrier. The two possible paths are intraband tunneling (I_{th}, thermionic current) and interband recombination or generation (I_{gen}, generation current). The latter can be divided into two processes, Shockley Read Hall (SRH) and Langevin recombination.

From the electrical characteristic of simple monolayer TMD field effect transistors, parameters like the free carrier mobility as well as threshold voltage (that correlates with the intrinsic doping) can be extracted. Such transistors are typically made by contacting the TMD flake exfoliated onto a SiO_2 covered Si wafer using two electrodes. The Si wafer functions as a back gate whereas, the SiO_2 layer serves as gate insulator and the TMD flake forms the channel of the transistor [43], [44]. The mentioned reports found that MoS_2 has an intrinsic n-type doping and a strong Fermi level pinning. Due to the strong Fermi level pinning, hole conduction can only be obtained by applying extremely strong gate fields. This could only be achieved by means of ionic liquid doping [45], [46]. Other than that, WSe_2 was found to be intrinsically un-doped. Using a split gate scheme therefore allowed to form a lateral p-n homojunction [26], [27].

The electrical characteristic of one of our devices is shown in Fig. 6(a). At a first glance the behavior could be described by the series connection of a WSe_2 and a MoS_2 transistor with an overlap that either forms a classical n-n junction (for gate

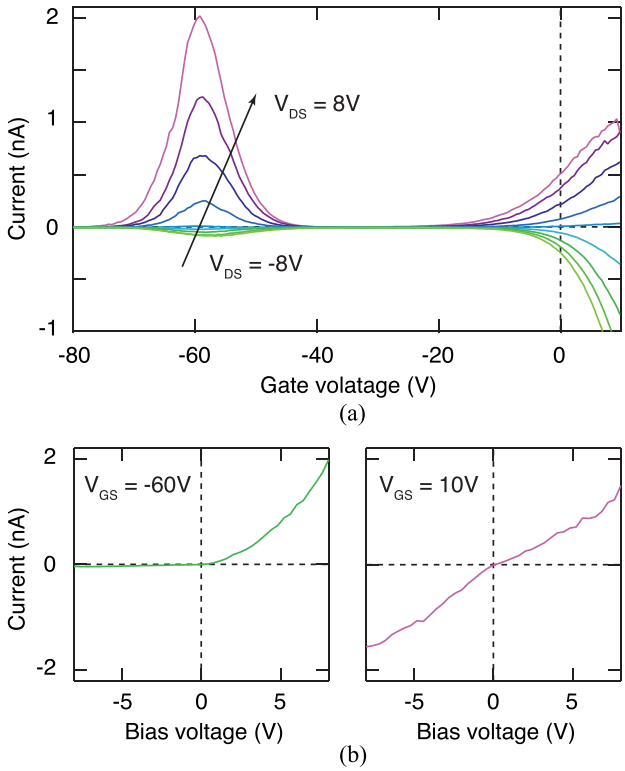

Fig. 6. Electrical characteristics of a dual bandgap device; (a) Gate voltage—current characteristics at different bias voltages. Two regions of distinct behavior appear at gate voltages $-75\,\mathrm{V} < \mathrm{V_G} < -40\,\mathrm{V}$ and $\mathrm{V_G} < -20\,\mathrm{V}$ that correspond to electrostatic p-n / n-n doping of the WSe_2-MoS_2 heterostructure. The applied bias voltages were: $-8, -6, -4, -2, 0, 2, 4, 6, 8$ V (green to lilac). (b) Rectifying and resistive behavior arising from different gate biasing ($V_G = -60$ V for the left plot, and $V_G = 10$ V for the right plot).

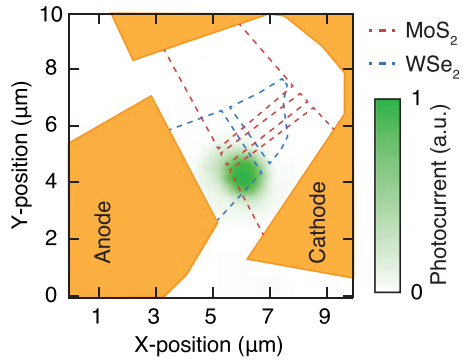

Fig. 7. Two-dimensional map of the short circuit current; The device outlines were overlaid on the measurement data for clarity. The position of the electrodes was verified by means of reflection intensity mapping. The orange areas indicate the electrodes, the WSe_2 flake is outlined by the blue dashed line, and the MoS_2 flake is outlined by the red dashed line.

voltages above 0 V), i-n junction (for gate voltages between 0 V and -50 V), p-n junction (for gate voltages between -50 and -70 V) or p-i junction (for gate voltages below -70 V). As the Fig. 6(b) and (c) show, the rectification behavior in the p-n case, and the resistive behavior in the n-n case would also suggest such a picture.

The typical measurement used to demonstrate an efficient conversion of optical into electrical energy is the solar cell current-voltage (I-V) curve. The applied bias voltage is scanned while measuring the current in darkness and under illumination. The so acquired data allow to extract various parameters that can then be used to model the cell using an equivalent circuit diagram. This again allows for a better understanding of the underlying physical processes. The I-V curves measured at illuminations with optical power densities ranging up to 640 mW/cm^2 are presented in Fig. 8(a). The inset of Fig. 8(a) shows the spectrum of our illumination source. A gate voltage of -50 V was applied for all the measurements. The shift of the I-V into the fourth quadrant confirms the power conversion. By connecting a load to the circuit an electrical power could be extracted. Ideally the load is chosen so that the cell operates at the maximum power point ($P_{\max}$, Fig. 8(b)).

A sketch explaining the processes that are the source for the power conversion is presented in Fig. 8(c). If the heterostructure is illuminated by a broadband source, photons that have energies larger than the optical bandgap of the respective material are absorbed. This either happens resonantly at the exciton energies or at energies above the electrical bandgap. Thus, the absorbed photons either directly form an exciton or thermalize to form one. The lowest energetic state in the heterostructure is given by its electrical bandgap ($E_{\mathrm{bg,HJ}}$). It is therefore obvious that if this energy is lower than the optical bandgap energies of the used materials, excitons are dissociated at the junction. If then the charge carriers do not form an interlayer exciton, charge separation happens. This is the source for a strong chemical potential energy gradient that drives the charge carriers in opposite direction to the contacts.

A photocurrent image was recorded by scanning a laser beam with a wavelength of 532 nm across the sample Fig. 7. The image clearly shows that the photocurrent is only generated in the contacted heterojunction area. This area is limited due to cracks in the TMD layers, indicated by dashed lines. The spatially resolved photocurrent measurement also demonstrates that the conversion does not originate from built-in fields. These fields can eventually be formed in proximity to the electrodes due to Schottky contacts.

The short circuit current (I_{SC}) and the open circuit voltage (V_{OC}) represent the case of no voltage produced between the electrodes and of no current flowing between the electrodes of the solar cell (see Fig. 8(a)). I_{SC} linearly depends on light intensity because of $G \propto \alpha P_{opt}$ [47]. Under steady state illumination, V_{OC} equals the difference between the electron and hole chemical potentials. As the free carrier density follows Fermi statistics V_{OC} can be expressed as

$$q\,V_{OC} = E_g - k_B T \,\ln \frac{N_C N_V}{n_e n_h} \qquad (1)$$

where *Eg* denotes the effective energy gap (the electric band gap of the heterojunction), k_{B} the Boltzmann constant, *T* the temperature, *N* the effective density of states of the conduction (c) and valence (v) band and *n* the free carrier concentration of electrons (e) and holes (h) [48]. In case of SRH recombination, free carriers recombine either trough a trap state or recombination center. As the density of these states does not depend on the light intensity, the following empirical relation holds for the recombination rate: $R \propto n_{trap} n(P_{opt})$. In case of Langevin recombination, generated carriers recombine with each other,

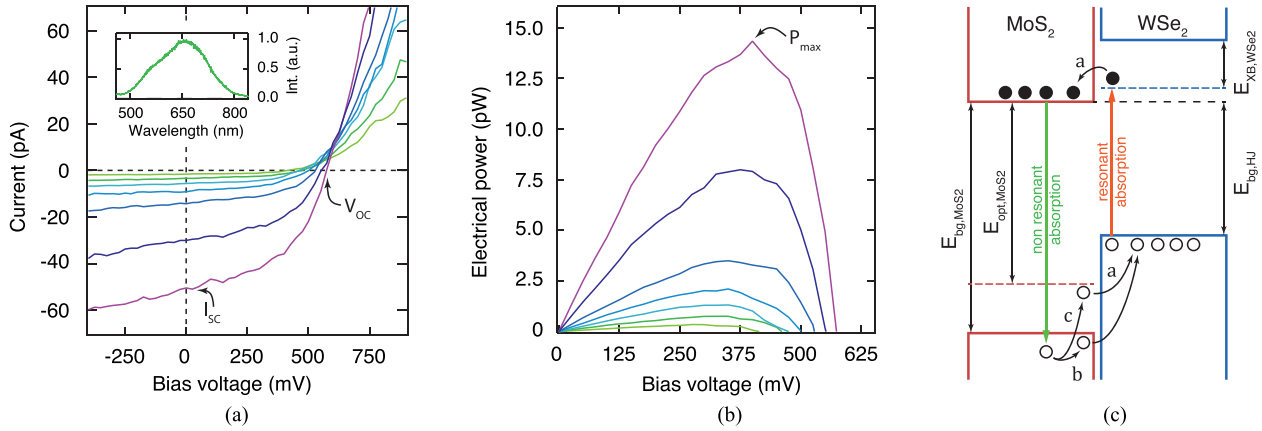

Fig. 8. Optical to electrical power conversion: (a) Solar cell I-Vs and (b) corresponding extracted electrical power at illumination intensities 18, 40, 67, 110, 180, 400, and 640 mW/cm^2. All measurements were performed at a gate voltage of −50 V. (c) Sketch of the power conversion process: Charge carriers are excited to higher energetic levels by resonant or non resonant absorption of a photon. In the case of resonant absorption an exciton is directly formed. Since a lower energetic level exists, the bound electron-hole pair dissociates at the interface (process a). Carriers excited to higher energetic levels by non resonant absorption either directly thermalize (process b) or bind to form an exciton (process c) and subsequently dissociate.

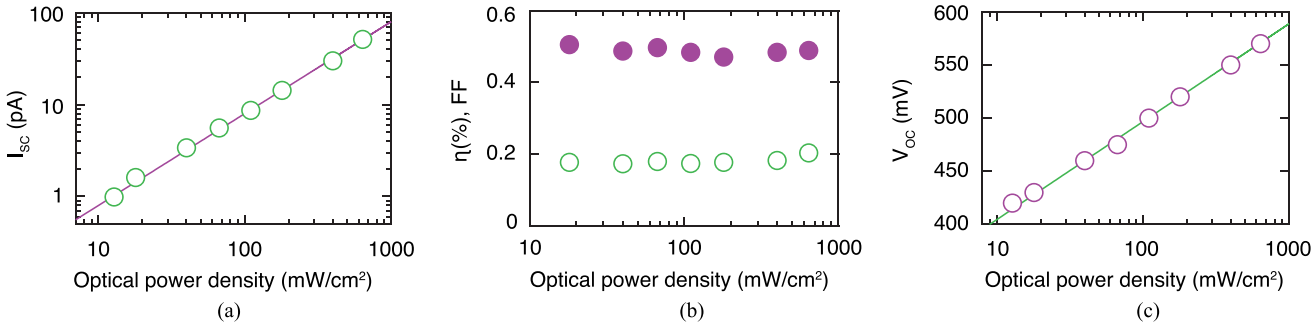

Fig. 9. Optical power density dependence of dual bandgap solar cell parameters: (a) Measured short circuit current (I_{SC}, green circles) and a linear fit according to theory (lilac line). (b) Intensity dependence of the fill factor (FF, filled lilac circles) and the power conversion efficiency (η, green circles). (c) Measured open circuit voltage (V_{OC}, lilac circles) along with a fit according to theory (green line).

thus the recombination rate is $R \propto n_e(P_{opt}) n_h(P_{opt})$ [49]. Under open circuit conditions, because no current flow is allowed, the generation rate equals the recombination rate. This results in a slope of $dV_{OC}/d\ln(P_{opt}) = 2 \cdot k_B T/q$ for SRH, and $dV_{OC}/d\ln(P_{opt}) = 1 \cdot k_B T/q$ for Langevin recombination. The slope found for our cell is 1.5 (see Fig. 9(a)) suggesting that both processes contribute to the recombination process.

The power conversion efficiency of a solar cell is defined as $\eta = P_{el}/P_{opt}$, where $P_{el} = \mathrm{FF}\ V_{OC}\ I_{SC}$ is the electrical power and FF the fill factor. Power dependent measurements of η and FF are presented in Fig. 9(b). We found an efficiency of about $\eta \approx 0.2\%$ for our double bandgap heterojuncion cells. This is in the same order of magnitude as the efficiency values reported for single layer WSe_2 homojunctions [26], [27]. The external quantum efficiency (EQE) is given by the ratio of generated carriers to impinging photons: $\mathrm{EQE} = [I_{SC}/q]/[P_{opt}/(hc/\lambda)]$ (h denotes Planck's constant, c speed of light and λ the wavelength ($\approx$ 590 nm). We found it to be $\approx 1.5\%$ in our devices (see linear fit in Fig. 9(c)).

To gain a deeper insight into the conversion process, we measured the photocurrent arising from an illumination of the junction area of our sample using two different laser sources. A 2.33 eV (532 nm) solid state laser was used to excite carriers to energies above the electrical band gaps of both materials (2.15 eV for MoS_2 and 2.08 eV for WSe_2) and the 1.65 eV (750 nm) laser was used to resonantly excite to the lowest exciton energy in WSe_2. As the heterostructure is made on a SiO_2 coated Si substrate, the effective optical intensity has a wavelength dependency due to interference $P_{opt,eff} = \kappa P_{opt}$. Taking this into account, the results plotted in Fig. 10(a) show similar behavior for both excitations. The presence of a photocurrent at 1.65 eV excitation suggests that the electrical band gap of the heterojunction is below the optical band gap of WSe_2. Thus, also the WSe_2 layer contributes to the conversion of photons into charge carriers. The rise of photocurrent that can be observed when increasing the excitation energy to 2.33 eV arises from the additional absorption in the MoS_2 layer. Furthermore, the lower saturation threshold observed for resonant excitation can be attributed to the lower cumulated density of states.

A type-II heterojunction is capable of efficiently dissociating excitons, and driving charge carriers to the electrodes even in opposition to a built-in electrical field [28]. The gate voltage dependent measurement of the short circuit current and open circuit voltage presented in Fig. 10(b) show this behavior. As

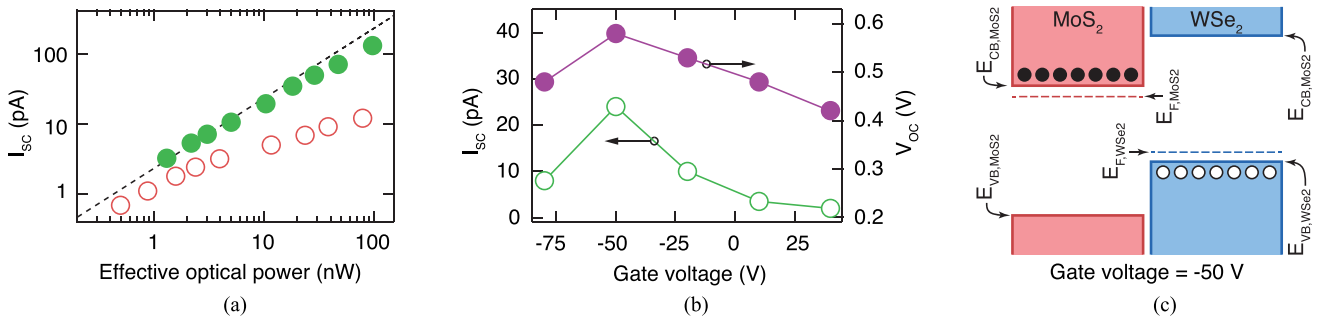

Fig. 10. (a) Short circuit currents (I_{SC}) arising from above bandgap excitation (filled green circles, 2.33 eV laser source), and resonant generation of excitons in WSe_2 (red circles, 1.85 eV laser source). The dashed line is a fit of $I_{SC} \propto P_{opt}$. (b) Gate voltage dependence of the short circuit current (I_{SC}, green circles) and open circuit voltage (V_{OC}, filled lilac circles). (c) Sketch of the Fermi level and band alignment at −50 V gate voltage.

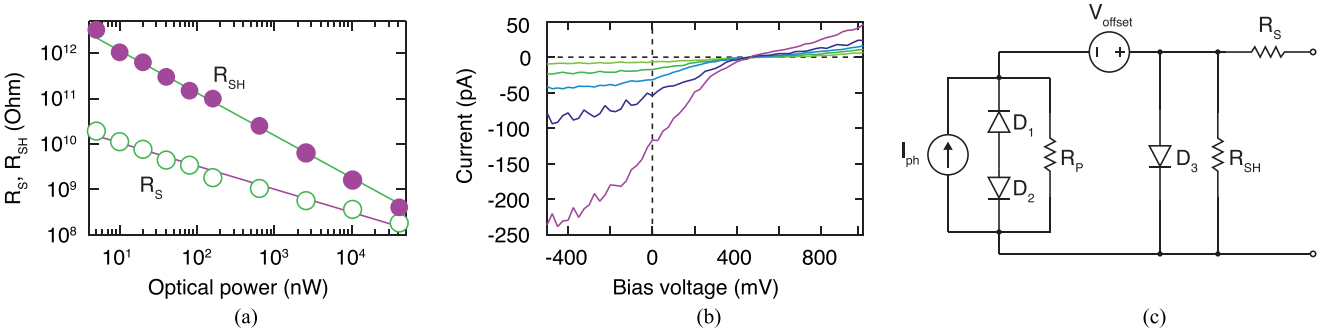

Fig. 11. (a) Illumination power dependence of the shunt (R_{SH}, filled lilac circles) and series (R_S, green circles) resistances. (b) S-shaped solar cell I-V with a kink at 400 mV measured at 167 K and illumination powers. (c) Equivalent circuit for solar cells with s-shaped I-Vs.

explained above, the junction in our devices can rather be seen as tunnel junction. Nevertheless, in case of a gate biasing of −50 V the quasi Fermi levels align such that the transport of charge carriers (holes in WSe_2 and electrons in MoS_2) is eased (see Fig. 10(c)).

The I-V characteristic of a conventional semiconductor solar cell can be modeled by a simple equivalent circuit scheme. An ideal cell is represented by a parallel circuit consisting of a current source (that drives the photogenerated current) and a diode. To represent a real cell a shunt resistance must be added in parallel (this accounts for the recombination losses) and a series resistance has to be added in series (to account for the losses due to contact resistance). At room temperature and low intensities (below 100 W/cm^2) we were able to extract these parameters. We found that the values extracted for the resistances changed upon an increase of illumination intensity (see Fig. 11(a)). The decrease of the cell's series resistance upon illumination can be attributed to the photogating of MoS_2. This happens as holes are trapped in the band tail states, present in MoS_2, due to structural defects in the layer or induced by disorder [50]. We suppose that the decrease of the shunt resistance may be attributed to a higher density of states leading to higher recombination losses. Additionally, we found that by rising the intensity level above 10 W/cm^2, a kink emerged around the maximum power point. This feature is often found in organic solar cells and commonly referred to as "s-shaped" I-V curve [51]. It strongly diminishes the FF and thus represents a strong reduction of the power conversion efficiency. Decreasing the cells temperature below room temperature lead to a more prominent appearance of this kink (see Fig. 11(b)). Thus, the equivalent circuit mentioned above has to be modified in order to obtain a proper model of the cell. Fig. 11(c) shows the model proposed by Sesa [52] for organic photovoltaic cells. As not only organic cells, but also hybrid (organic/TMD) cells [53] as well as van der Waals heterostructures show this s-shaped I-V characteristic, we suspect that the kink is due to the excitonic nature of these photovoltaic devices. We therefore suggest that the model proposed by Sesa should be applied for a description of the behaviour of cells in which the photocurrent generation relies on high exciton binding energies combined with type-II heterostructures. An extraction of the model-fit parameters across the full range of the I-V curve would be of use to identify the underlying physical processes but requires additional measurements on large number of devices. For now we suspect that the kink arises because of a blocking of one species of charge carriers, formed by exciton dissociation, at one contact.

B. Triple Bandgap Heterostructure

In principle, triple bandgap heterostructures should allow for a more efficient harvesting of the solar spectrum by the introduction of a material with a larger bandgap. The electrical characteristic of our triple bandgap heterostructure is presented in Fig. 12(a). Similar to the results found for double bandgap heterostructures two distinct regimes appeared. The WS_2 bands are expected to align such that the conduction and valence band-

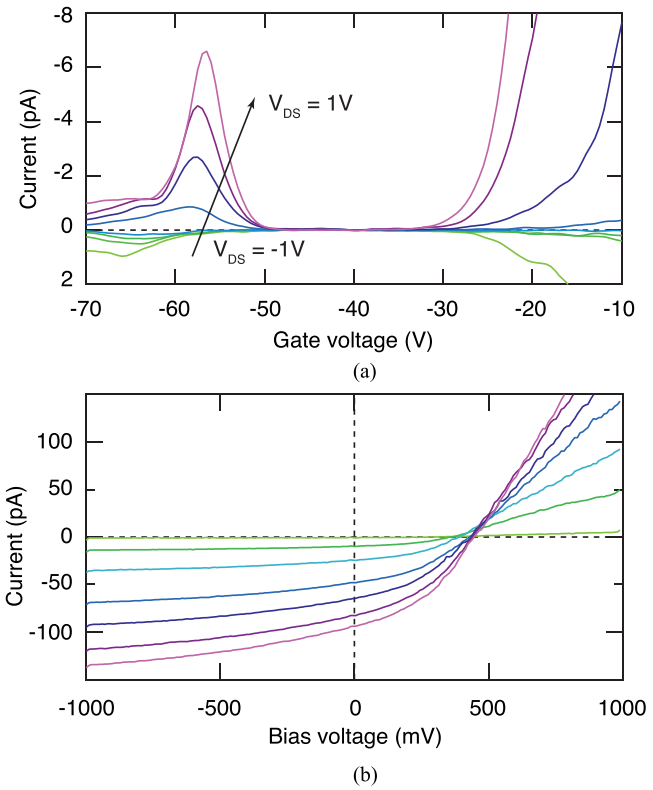

Fig. 12. Electrical and photovoltaic characteristics of a triple bandgap device: (a) Gate voltage—current characteristic at different bias voltages. Again two regions of distinct behavior evolve at gate voltages $-65\ \mathrm{V} < \mathrm{V_G} < -50\ \mathrm{V}$ and $\mathrm{V_G} < -30\ \mathrm{V}$ that correspond to electrostatic p-n / n-n doping of the WSe_2-MoS_2 heterostructure. The applied bias voltages were: -1, -0.75, -0.5, -0.25, 0, 0.25, 0.5, 0.75, and 1 V (green to lilac line). (b) Solar cell I-Vs at illumination intensities: 20, 320, 640, 1180, 1520, 1900, and 2200 mW/cm^2 (green to lilac line).

edge are found in-between the respective band edges in MoS_2 and WSe2 [29], [30]. WS_2, like WSe_2, is known to be intrinsically undoped. Thus, we expect the impact of the gate voltage on the Fermi level in this layer to be similar to the what was observed for WSe_2. In this triple bandgap heterostructure, the region at a gate voltage around -65 V leads to a p-p-n junction and above -20 V, a n-n-n junction is formed. It should be noted that a precise alignment of the energetic levels is far harder to sketch for a triple bandgap heterostructure. This, because the increased screening of the gate voltage, due to the charge carrier concentration in the WS_2 layer, introduces an additional degree of freedom. Fig. 12(b) shows that an efficient photovoltaic effect arises upon illumination of the heterostructure. Again, two-dimensional photocurrent maps were acquired to ensure that the photocurrent indeed stems from the heterojunction area. The I-V again allows to calculate the power conversion efficiency of $\eta \approx 0.1\%$.

Comparing these results with the values found for double bandgap cells shows no increase in power conversion efficiency. Thus, we suspect that the effective electrical heterojunction bandgap ($\mathrm{E_{bg,HJ}}$) did not change. This again indicates that van der Waals heterostructures have to be considered as excitonic solar cells. Unlike in semiconductor solar cells, the optical and electrical bandgaps differ in such cells. The optical bandgaps control the light absorption, whereas the effective electrical bandgap of the heterojunction (see Fig. 8(c) $E_{\mathrm{bg,HJ}}$) determines the standard free energy of generated electron-hole pairs [28]. The excitons are only dissociated at the junction if the electrical bandgap of the heterojunction ($E_{\mathrm{bg,HJ}}$) is smaller than the exciton energy ($E_{\mathrm{opt}} = E_{\mathrm{bg}} - E_{\mathrm{x}}$). This gives a charge-separation threshold ($E_{\mathrm{bg,HJ}} \leq E_{\mathrm{opt}}$) [33]. In the ideal case the optical bangap of the materials equals the electrical bandgap of the heterojunction.

IV. Conclusion

We presented a detailed description of two fabrication processes used for the fabrication of van der Waals heterostructures. Using these processes, two different types of photovoltaic devices were realized—a double bandgap and a triple bandgap van der Waals solar cell. Both devices convert optical into electrical power. The power conversion efficiency for both cells was found to be of the same order of magnitude (0.1 to 0.2%), in agreement with predicted values [19]. We found that SRH and Langevin recombination coexist in our devices. A model for the electric properties and a schematic model that reproduces the s-shaped I-V curve at high illumination intensities were proposed.

Van der Waals heterostructures can be formed without worrying about lattice matching of the single materials, which eases the formation of a multi bandgap solar cell. The ideal band gaps for a cell made by a stack of two materials with 100% absorption are calculated to be 0.94 and 1.6 eV. For a triple bandgap solar cell the ideal values are found to be 0.94, 1.37 and 1.90 eV [54]. The wide range of band gaps found in commonly used semiconducting TMDs suggests that such a multi bandgap cell could be made. The results of our measurements on the triple bandgap cell are a strong indication that excitonic processes play a major role in the photovoltaic effect of van der Waals heterostructures. Our findings show that for enhancing the efficiency of multi bandgap cells a scheme different to the one used in our triple bandgap devices has to be applied. We envision that a stack of multiple double bandgap van der Waals heterostructures, separated by a few layer thick barrier of hexagonal boron nitride, could indeed be used to increase the power conversion efficiency. Such a structure would still be rather simple and avoids the need for complex spectral splitting setups that need to be applied for an optimization of multiple bandgap cells made of III-V and IV semiconductors [55].

Recently published work on heterostructures made by combining two TMD layers [30], [56], [57], one TMD layer and one layer of black phosphorus [58], one TMD layer and a conventional semiconductor [59], as well as one TMD layer and an organic semiconductor [53], [60] shows results similar to our report. It must be noted that even for a structure composed of two TMD layers, the reported external quantum efficiency values span from 0.1% [56] to 12% [61]. We suggest that this strong variation can probably be attributed to differences in fabrication and/or materials. However, the reported measurements match from a qualitative point of view.

When comparing the efficiencies we reported in this work with other cells, it must be kept in mind that the quality of

the used materials is still rather poor. It was recently shown that by improving the stoichiometry using a superacid strongly improved the photoluminescence quantum yield of MoS_2. Increasing the ratio of 1.84:1 (S:Mo) in the exfoliated flake to 1.95:1 in the chemically treated flake allowed to enhance the photoluminescence by more than two orders of magnitude [62]. We demonstrated that defects strongly contribute to the recombination losses in our cells. This suggests that that an improved crystal stoichiometry will lead to a rise in photoconversion efficiency of van der Waals heterostructures. One further bottle neck for the development of commercial van der Waals heterostructure solar cells is the lack of large area TMD crystals. The large effort currently put into the growth of such TMD layers could solve both mentioned problems.

It is expected that module costs play a major role for upcoming generations of solar cells [63]. From this perspective van der Waals heterostructures seem promising candidates. The amount of raw material needed for the active region is minimal, also the power conversion densities are expected to be orders of magnitude higher than in conventional cells. TMD based solar cells can easily be combined with methods for efficiency enhancement [64], [65], and their exitonic character eventually allows to strongly increase the efficiency by a design of the exitonic dark states [20].

ACKNOWLEDGMENT

The authors would like to thank G. Kresse, K. Hummer, J. Burgdörfer, F. Libisch, and K. Unterrainer for valuable discussions; M. Schinnerl, G. D. Cole, and M. Glaser for technical assistance; E. Bertagnolli and A. Lugstein for providing access to a Raman spectrometer.

REFERENCES

[1] R. F. Frindt, "Optical absorption of a few unit-cell layers of MoS2," *Phys. Rev.*, vol. 140, no. 2A, pp. A536–A539, Oct. 1965.

[2] R. F. Frindt and A. D. Yoffe, "Physical properties of layer Structures: Optical properties and photoconductivity of thin crystals of molybdenum disulphide," in *Proc. Roy. Soc. London A, Math. Phys. Eng. Sci.*, vol. 273, no. 1352, pp. 69–83, Apr. 1963.

[3] A. Clark and R. H. Williams, "The optical absorption properties of synthetic MoS2," *J. Phys. D, Appl. Phys.*, vol. 1, no. 9, pp. 1222–1224, Dec. 1968.

[4] H. I. Ralph, "The electronic absorption edge in layer type crystals," *Solid State Commun.*, vol. 3, no. 10, pp. 303–306, Oct. 1965.

[5] J. A. Wilson and A. D. Yoffe, "The transition metal dichalcogenides discussion and interpretation of the observed optical, electrical and structural properties," *Adv. Phys.*, vol. 18, no. 73, pp. 193–335, May 1969.

[6] G. Kline, K. Kam, D. Canfield, and B. A. Parkinson, "Efficient and stable photoelectrochemical cells constructed with WSe2 and MoSe2 photoanodes," *Solar Energy Mater.*, vol. 4, no. 3, pp. 301–308, Mar. 1981.

[7] E. Fortin and W. M. Sears, "Photovoltaic effect and optical absorption in MoS2," *J. Phys. Chem. Solids*, vol. 43, no. 9, pp. 881–884, Jan. 1982.

[8] C. Clemen, X. I. Saldaña, and P. Munz, "Photovoltaic properties of some semiconducting layer structures," *Physica Status Solidi (a)*, vol. 49, no. 2, pp. 437–443, 1978.

[9] A. Koma, K. Sunouchi, and T. Miyajima, "Fabrication and characterization of heterostructures with subnanometer thickness," *Microelectron. Eng.*, vol. 2, no. 1–3, pp. 129–136, Oct. 1984.

[10] A. Koma, K. Saiki, and Y. Sato, "Heteroepitaxy of a two-dimensional material on a three-dimensional material," *Appl. Surface Sci.*, vol. 41/42, pp. 451–456, Apr. 1989.

[11] A. Koma, "Van der Waals epitaxy—A new epitaxial growth method for a highly lattice-mismatched system," *Thin Solid Films*, vol. 216, no. 1, pp. 72–76, Aug. 1992.

[12] T. Tsirlina *et al.*, "Growth of crystalline WSe2 and WS2 films on amorphous substrate by reactive (Van der Waals) rheotaxy," *Solar Energy Mater. Solar Cells*, vol. 44, no. 4, pp. 457–470, Dec. 1996.

[13] K. S. Novoselov, A. K. Geim, S. V. Morozov, and D. Jiang, "Electric field effect in atomically thin carbon films," *Science*, vol. 306, pp. 666–669, Oct. 2004.

[14] K. S. Novoselov *et al.*, "Two-dimensional atomic crystals," *Proc. Nat. Acad. Sci. USA*, vol. 102, no. 30, pp. 10 451–10 453, Jul. 2005.

[15] A. Pospischil and T. Mueller, "Optoelectronic devices based on atomically thin transition metal dichalcogenides," *Appl. Sci.*, vol. 6, no. 3, p. 78, Mar. 2016.

[16] K. F. Mak, C. Lee, J. Hone, J. Shan, and T. F. Heinz, "Atomically thin MoS2: A new direct-gap semiconductor," *Phys. Rev. Lett.*, vol. 105, no. 13, Sep. 2010, Art. no. 136805.

[17] A. Chernikov *et al.*, "Exciton binding energy and nonhydrogenic rydberg series in monolayer WS2," *Phys. Rev. Lett.*, vol. 113, no. 7, Aug. 2014, Art. no. 076802.

[18] D. K. Zhang, D. W. Kidd, and K. Varga, "Excited biexcitons in transition metal dichalcogenides," *Nano Lett.*, vol. 15, no. 10, pp. 7002–7005, Oct. 2015.

[19] M. Bernardi, M. Palummo, and J. C. Grossman, "Extraordinary sunlight absorption and one nanometer thick photovoltaics using two-dimensional monolayer materials," *Nano Lett.*, vol. 13, no. 8, pp. 3664–3670, Jul. 2013.

[20] Y. Yamada, Y. Yamaji, and M. Imada, "Exciton lifetime paradoxically enhanced by dissipation and decoherence: Toward efficient energy conversion of a solar cell," *Phys. Rev. Lett.*, vol. 115, no. 19, Nov. 2015, Art. no. 197701.

[21] U. Aeberhard, "Simulation of ultra-thin solar cells beyond the limits of the semi-classical bulk picture," *IEEE J. Photovolt.*, vol. 6, no. 3, pp. 654–660, Nov. 2015.

[22] D. Mozyrsky and I. Martin, "Efficiency of thin film photocells," *Opt. Commun.*, vol. 277, no. 1, pp. 109–113, Sep. 2007.

[23] W. Yang, "Ultra-thin GaAs single-junction solar cells integrated with a reflective back scattering layer," *J. Appl. Phys.*, vol. 115, no. 20, May 2014, Art. no. 203105.

[24] A. D. Martinez *et al.*, "Solar energy conversion properties and defect physics of ZnSiP2," *Energy Environ. Sci.*, vol. 9, pp. 1031–1041, Jan. 2016.

[25] S. J. Fonash, *Solar Cell Device Physics*. Amsterdam, The Netherlands: Elsevier, 2010.

[26] A. Pospischil, M. M. Furchi, and T. Mueller, "Solar-energy conversion and light emission in an atomic monolayer p–n diode," *Nature Nanotechnol.*, vol. 9, no. 4, pp. 257–261, Mar. 2014.

[27] B. W. H. Baugher, H. O. H. Churchill, Y. Yang, and P. Jarillo-Herrero, "Optoelectronic devices based on electrically tunable p–n diodes in a monolayer dichalcogenide," *Nature Nanotechnol.*, vol. 9, no. 4, pp. 262–267, Mar. 2014.

[28] B. A. Gregg, "The photoconversion mechanism of excitonic solar cells," *MRS Bull.*, vol. 30, no. 01, pp. 20–22, 2005.

[29] J. Kang, S. Tongay, J. Zhou, J. Li, and J. Wu, "Band offsets and heterostructures of two-dimensional semiconductors," *Appl. Phys. Lett.*, vol. 102, no. 1, 2013, Art. no. 012111.

[30] C. Gong *et al.*, "Band alignment of two-dimensional transition metal dichalcogenides: Application in tunnel field effect transistors," *Appl. Phys. Lett.*, vol. 103, no. 5, 2013, Art. no. 053513.

[31] A. Splendiani *et al.*,"Emerging photoluminescence in monolayer MoS2," *Nano Lett.*, vol. 10, no. 4, pp. 1271–1275, Mar. 2010.

[32] P. Tonndorf *et al.*,"Photoluminescence emission and Raman response of monolayer MoS2, MoSe2, and WSe2," *Opt. Express*, vol. 21, no. 4, pp. 4908–4916, Feb. 2013.

[33] A. C. Morteani, P. Sreearunothai, L. M. Herz, R. H. Friend, and C. Silva, "Exciton regeneration at polymeric semiconductor heterojunctions," *Phys. Rev. Lett.*, vol. 92, no. 24, Jun. 2004, Art. no. 247402.

[34] Z. Cheng *et al.*,"Toward intrinsic graphene Surfaces: A systematic study on thermal annealing and wet-chemical treatment of SiO2-supported graphene devices," *Nano Lett.*, vol. 11, no. 2, pp. 767–771, Jan. 2011.

[35] A. Uhl, J. Bendig, J. Leistner, U. A. Jagdhold, and J. J. Bauer, "E-beam and deep-UV exposure of PMMA-based resists: Identical or different chemical behavior?" in *Proc. 23rd Annu. Int. Symp. Microlithography*, Jun. 1998, vol. 3333, pp. 1452–1457.

[36] W. Zhao *et al.*, "Evolution of electronic structure in atomically thin sheets of WS2 and WSe2," *ACS Nano*, vol. 7, no. 1, pp. 791–797, Dec. 2012.

[37] M. A. Meitl *et al.*, "Transfer printing by kinetic control of adhesion to an elastomeric stamp," *Nat. Mater.*, vol. 5, no. 1, pp. 33–38, Dec. 2005.

[38] L. Li *et al.*, "Nanofabrication on unconventional substrates using transferred hard masks," *Sci. Rep.*, vol. 5, Jan. 2015, Art. no. 7802.
[39] C. Zhang, A. Johnson, C.-L. Hsu, L.-J. Li, and C.-K. Shih, "Direct imaging of band profile in single layer MoS 2on graphite: Quasiparticle energy gap, metallic edge states, and edge band bending," *Nano Lett.*, vol. 14, no. 5, pp. 2443–2447, May 2014.
[40] H. Heo *et al.*, "Interlayer orientation-dependent light absorption and emission in monolayer semiconductor stacks," *Nature*, vol. 6, 2015, Art. no. 7372.
[41] P. Rivera *et al.*, "Observation of long-lived interlayer excitons in monolayer MoSe2–WSe2 heterostructures," *Nature Commun.*, vol. 6, Feb. 2015, Art. no. 6242.
[42] H. Fang *et al.*, "Strong interlayer coupling in van der Waals heterostructures built from single-layer chalcogenides," *Proc. Nat. Acad. Sci. USA*, vol. 111, no. 17, pp. 6198–6202, Apr. 2014.
[43] B. Radisavljevic, A. Radenovic, J. Brivio, V. Giacometti, and A. Kis, "Single-layer MoS2 transistors," *Nature Nanotechnol.*, vol. 6, no. 3, pp. 147–150, Jan. 2011.
[44] S. Das, H.-Y. Chen, A. V. Penumatcha, and J. Appenzeller, "High performance multilayer MoS2 transistors with scandium contacts," *Nano Lett.*, vol. 13, no. 1, pp. 100–105, Dec. 2012.
[45] Y. Zhang, J. Ye, Y. Matsuhashi, and Y. Iwasa, "Ambipolar MoS2 thin flake transistors ," *Nano Lett.*, vol. 12, no. 3, pp. 1136–1140, 2012.
[46] M. M. Perera *et al.*, "Improved carrier mobility in few-layer MoS 2 field-effect transistors with ionic-liquid gating," *ACS Nano*, vol. 7, no. 5, pp. 4449–4458, 2013.
[47] D. Cheyns *et al.*, "Analytical model for the open-circuit voltage and its associated resistance in organic planar heterojunction solar cells," *Phys. Rev. B.*, vol. 77, no. 16, Apr. 2008, Art. no. 165332.
[48] G. Garcia-Belmonte, "Temperature dependence of open-circuit voltage in organic solar cells from generation-recombination kinetic balance," *Solar Energy Mater. Solar Cells*, vol. 94, no. 12, pp. 2166–2169, Dec. 2010.
[49] S. R. Cowan, A. Roy, and A. J. Heeger, "Recombination in polymer-fullerene bulk heterojunction solar cells," *Phys. Rev. B.*, vol. 82, no. 24, Dec. 2010, Art. no. 245207.
[50] M. M. Furchi, D. K. Polyushkin, A. Pospischil, and T. Mueller, "Mechanisms of photoconductivity in atomically thin MoS2," *Nano Lett.*, vol. 14, no. 11, pp. 6165–6170, Oct. 2014.
[51] W. Tress, S. Pfuetzner, K. Leo, and M. Riede, "Open circuit voltage and IV curve shape of ZnPc:C60 solar cells with varied mixing ratio and hole transport layer," *J. Photon. Energy*, vol. 1, no. 1, pp. 011 114–011 114– 11, Jan. 2011.
[52] E. Sesa, "A novel electrical model for organic photovoltaic cells," Ph.D. dissertation, Faculty of Sci. & Inform. Technol., School of Mathe. and Phys. Sci., Univ. of Newcastle, NSW, Austrailia, Aug. 2013.
[53] D. He *et al.*, "A van der Waals pn heterojunction with organic/inorganic semiconductors," *Appl. Phys. Lett.*, vol. 107, no. 18, Nov. 2015, Art. no. 183103.
[54] S. P. Bremner, M. Y. Levy, and C. B. Honsberg, "Analysis of tandem solar cell efficiencies under AM1.5G spectrum using a rapid flux calculation method," *Progress Photovoltaics: Res. Appl.*, vol. 16, no. 3, pp. 225–233, May 2008.
[55] C. Maragliano *et al.*, "Demonstration of a novel dispersive spectral splitting optical element for cost-effective photovoltaic conversion," unpublished paper, Aug. 2015. [Online]. Available: http://arxiv.org/abs/1508.00210.
[56] Y. Gong *et al.*, "Two-step growth of two-dimensional WSe2/MoSe2 heterostructures," *Nano Lett.*, vol. 15, no. 9, pp. 6135–6141, Aug. 2015.
[57] C.-H. Lee *et al.*, "Atomically thin p–n junctions with van der Waals heterointerfaces," *Nature Nanotechnol.*, vol. 9, no. 9, pp. 676–681, Sep. 2014.
[58] Y. Deng *et al.*, "Black phosphorus–monolayer MoS2 van der Waals heterojunction p–n Diode," *ACS Nano*, vol. 8, no. 8, pp. 8292–8299, Jul. 2014.
[59] O. Lopez-Sanchez *et al.*, "Light generation and harvesting in a van der Waals heterostructure," *ACS Nano*, vol. 8, no. 3, pp. 3042–3048, Mar. 2014.
[60] S. Vélez *et al.*, "Gate-tunable diode and photovoltaic effect in an organic–2D layered material p–n junction," *Nanoscale*, vol. 7, no. 37, pp. 15 442–15 449, Sep. 2015.
[61] R. Cheng *et al.*, "Electroluminescence and photocurrent generation from atomically sharp WSe2 / MoS2 heterojunction p–n diodes," *Nano Lett.*, vol. 14, no. 10, pp. 5590–5597, Oct. 2014.
[62] M. Amani *et al.*, "Near-unity photoluminescence quantum yield in MoS2," *Science*, vol. 350, no. 6264, pp. 1065–1068, Nov. 2015.
[63] M. C. Beard, J. M. Luther, and A. J. Nozik, "The promise and challenge of nanostructured solar cells," *Nature Nanotechnol.*, vol. 9, no. 12, pp. 951–954, Dec. 2014.
[64] S. V. Boriskina and G. Chen, "Exceeding the solar cell Shockley–Queisser limit via thermal up-conversion of low-energy photons," *Opt. Commun.*, vol. 314, pp. 71–78, Mar. 2014.
[65] J. Zheng, R. A. Barton, and D. Englund, "Broadband coherent absorption in chirped-planar-dielectric cavities for 2D-material-based photovoltaics and photodetectors," *ACS Photon.*, vol. 1, no. 9, pp. 768–774, Sep. 2014.

Marco M. Furchi received the B.S. degree in electrical engineering and the M.S. degree in microelectronics both from Vienna University of Technology, Wien, Austria, in 2009 and 2012, respectively. He is currently working toward the Ph.D. degree at the Photonics Institute of TU Wien, Vienna, Austria. His current research interests include optical and electrical properties of graphene and atomically thin transition metal dichalcogenides.

Armin A. Zechmeister received the M.S. degree in physical energy and measurement engineering from the Photonics Institute, Vienna University of Technology, Vienna, Austria, in 2015. He was working on novel technologies based on two-dimensional semiconductors applied to solar energy harvesting.

Florian Hoeller received the M.S. degree in electrical engineering from the Vienna University of Technology, Vienna, Austria, in 2015. He is currently with automation industries and is highly interested in solid-state physics and light-matter interaction phenomena. His university research was mainly about time and frequency resolved laser spectroscopy of 2-D materials.

Stefan Wachter received the M.Sc. degree in electrical engineering from Technische Universität Wien, Wien, Austria, in 2014. He is currently working toward the Ph.D. degree at the Photonics Institute, Vienna University of Technology, Vienna, Austria. His research interest includes excitonic light emission in two-dimensional heterostructures.

Andreas Pospischil received the Ph.D. degree from the Vienna University of Technology, Vienna, Austria, and is now a Postdoctoral Researcher at the Photonics Institute, Vienna University of Technology. His research interests include generation and detection of light in atomically thin transition metal dichalcogenides.

Thomas Mueller received the M.Sc. and Ph.D. degrees in electrical engineering from the Vienna University of Technology, Vienna, Austria, in 2001 and 2004, respectively. His Ph.D. work focused on terahertz spectroscopy of nanostructures. He then was a University Assistant at the Vienna University of Technology from 2005 to 2007. In 2007, he joined the IBM Thomas J. Watson Research Center, Yorktown Heights, NY, USA, as a Postdoctoral Researcher, where he worked on carbon-based electronics. End of 2009, he returned to Vienna, where he currently holds an Assistant Professor position. His research interests include photonics and electronics using graphene and other two-dimensional materials. He authored and (co-)authored more than 65 peer-reviewed publications in leading scientific journals. He received the START-Prize, the Fritz Kohlrausch-Prize, and the ASciNA Award.